Title

Fast parametric relationships for the large-scale reservoir simulation of mixed CH4-CO2 gas hydrate systems

Authors

Reagan, Matthew T
Moridis, George J
Seim, Katie S

Publication Date

2017-06-01

DOI

10.1016/j.cageo.2017.03.018

Peer reviewed

Fast Parametric Relationships for the Large-Scale Reservoir Simulation of Mixed CH_4-CO_2 Gas Hydrate Systems

Matthew T. Reagan* (mtreagan@lbl.gov), George J. Moridis (gjmoridis@lbl.gov),
Katie S. Seim
Earth and Environmental Science Area,
Energy Geosciences Division,
Lawrence Berkeley National Laboratory
1 Cyclotron Rd.
Berkeley, CA 94720

*Corresponding author

Abstract

A recent Department of Energy field test on the Alaska North Slope has increased interest in the ability to simulate systems of mixed CO_2-CH_4 hydrates. However, the physically realistic simulation of mixed-hydrate simulation is not yet a fully solved problem. Limited quantitative laboratory data leads to the use of various *ab initio*, statistical mechanical, or other mathematic representations of mixed-hydrate phase behavior. Few of these methods are suitable for inclusion in reservoir simulations, particularly for systems with large number of grid elements, 3D systems, or systems with complex geometric configurations. In this work, we present a set of fast parametric relationships describing the thermodynamic properties and phase behavior of a mixed methane-carbon dioxide hydrate system. We use well-known, off-the-shelf hydrate physical properties packages to generate a sufficiently large dataset, select the most convenient and efficient mathematical forms, and fit the data to those forms to create a physical properties package suitable for inclusion in the TOUGH+ family of codes. The mapping of the phase and thermodynamic space reveals the complexity of the mixed-hydrate system and allows understanding of the thermodynamics at a level beyond what much of the existing laboratory data and literature currently offer.

Keywords

Methane hydrate, CO2 hydrate, mixed hydrate, equation of state

51 1. Introduction

52 1.1 Sequestration of CO2 in hydrate-bearing reservoirs

53

54 The Ignik Sikumi field test (Schoderbek et al. 2013), performed in 2012, attempted to test
55 the process of CO_2 sequestion in combination with natural gas production from methane
56 hydrates. The objective was to establish whether such exchange-reaction sequestion is viable and
57 determine how such a process can be implemented at the field scale. The field trial was
58 performed by ConocoPhillips and the Japan Oil, Gas, and Metals National Co. (JOGMEC) on
59 behalf of the Department of Energy. In anticipation of the test, several institutions have
60 performed lab and theoretical investigations of the properties of mixed hydrates.

61 Previous research (Hester et al., 2011a; Howard, et al., 2011) had established the process
62 by which injection of CO_2 into methane hydrate-bearing sediments can 1) sequester CO_2 as CO_2-
63 hydrate, and 2) release free gaseous CH_4 into the reservoir in such a way that it can be produced
64 commercially. Such exchange of CO_2 for CH_4 would provide a nearly one-for-one process of
65 exchanging previously emitted carbon for new, cleaner fossil-fuel resources. However, the
66 ability to simulate such systems is currently limited. Previous work in the commercialization of
67 methane hydrates has depended heavily on numerical simulation capabilities (Moridis et al.,
68 2011), but currently mixed-hydrate systems are served by a limited number of simulation tools.

69 A key hint about the nature of the mixed CO_2-CH_4 system comes from legacy cryonics
70 literature. Donnelly and Katz (1954) generated a phase diagram for the mixed system with a
71 noted focus on cryogenic properties, however, the higher-*T* end of their phase diagram, although
72 low resolution and derived from a minimal number of data points, hints at a key insight into
73 mixed systems. Instead of a critical point, such systems have a *critical locus*, whereby the critical

74 point of the *mixture* varies with composition. For this system in particular, the critical locus
75 appears to pass through the *P*-*T* region associated with hydrate formation, and in particular, the
76 region in which a CO_2-CH_4 exchange reaction will occur. This key insight warns that
77 supercritical behaviors, for example, transitions from liquid to gas phases without a phase
78 transition (assuming the correct path is taken in *P*-*T* space) may be considered, and that
79 formation of a second liquid-CO_2 phase (appearing and disappearing as temperatures change
80 between injection, re-equilibration, and production) may be a common occurrence during many
81 injection-production strategies.
82 The existence of a CO_2-CH_4 exchange reaction that occurs on days-to-weeks timescales
83 has been confirmed in the lab (Hester et al., 2011a; Howard, et al., 2011), although quantitative
84 measures of actual thermodynamic properties (i.e., *P*-*T* curves) were will beyond the scope of
85 such work. The bulk of our knowledge comes from theoretical studies, that use *ab initio*, or
86 statistical mechanical (statistical thermodynamic) methods—most notably a number of papers by
87 Trout, Anderson, and Cao (Anderson, et al., 2007; Garapati et al., 2011), which develop a model
88 using the methods proposed by van der Waals and Platteeuw (1959). A more accessible system
89 for understanding pure and mixed hydrates was published with the seminal text on hydrates by
90 Sloan and Koh (2008). CSMGem uses the Gibbs Free Energy minimization method (GEM)
91 (Gupta, 1990; Ballard, 2002; 2004) to estimate a wide range of physical properties for complex
92 hydrate systems over a wide range of conditions. Preliminary studies using both CSMGem and
93 lab data have shown evidence of good agreement (Luzi et al., 2012).
94 White and collaborators at PNNL (White and Oostrom, 2006; White, et al., 2011) created
95 the first comprehensive mixed-hydrate simulator by incorporating CO_2 injection processes in the
96 STOMP family of simulation codes. This implementation used lookup tables derived from

previously referenced theoretical work, but did not include some of the complex thermodynamics described in detail later in this paper. The goal of this continuing work is to implement additional necessary complexity within the framework of a general-purpose reservoir simulator.

1.2 Requirements for reservoir simulation

While previous reservoir simulation studies have used lookup tables derived from other data sources (notably TOUGH2-ECO2M, in Pruess, 2011), this approach is less desirable as reservoir simulation moves into more sophisticated terrain, representing larger systems (100,000s to 1,000,000s of gridblocks), three-dimensional geometries, and systems involving steep gradients and complex thermodynamics. A fully implicit reservoir simulator such as TOUGH+ may not only need to solve 10,000,000 equations at each timestep, but also engage in 2-10 Newton-Raphson iterations as well, with each iteration requiring a complete update of element-by-element and connection-by-connection properties. The slowness of interpolating values off a lookup table is likely to severely restrict the scope and size of such a simulation. If an extensive and detailed set of empirical data were available, there could be an acceptable tradeoff between speed and accuracy, but at the current time no such dataset exists for mixed CH_4-CO_2 hydrates at the reservoir conditions of interest. Therefore, it is reasonable to use limited data, statistical mechanics, or *ab initio*-generated data to create efficient functional expressions for physical properties, since any inaccuracies allowed by the function form are proportional to the natural uncertainty of the underlying data (as long as this is acknowledged in the presentation of the results).

120 An additional issue is that of functional smoothness and continuity. Although it is simple
121 to create visually smooth functions using any number of methods, the actual numerical
122 smoothness of the function, and its derivatives, is absolutely crucial to the formulation of the
123 numerical problem. For Jacobian-based numerical formulation, such as used by TOUGH+, the
124 functions and their derivatives must be smooth and continuous. By careful selection of
125 appropriate functional forms, these properties can be guaranteed.
126 This paper is the first in a series describing the formulation of the TOUGH+BinH code.
127 A subsequent publication will describe how these physical properties relationships to the
128 construction of a new TOUGH+ "equation of state" module (i.e., the specific software package
129 that describes phase transitions and computes evolving phase saturations and compositions for a
130 given set of components and *PVTx* conditions) and the testing of the new simulator with 1-D and
131 2-D sample problems.
132
133 2. Methods
134 2.1 GSMGem
135
136 To provide a source for *P*-*T*-*x* data for the mixed CH_4-CO_2 system, in the absence of a
137 library of high-resolution data, we use CSMGem, the application published with the seminal text
138 on hydrates by Sloan and Koh (2008). CSMGem uses the Gibbs Free Energy minimization
139 method (GEM) (Gupta, 1990; Ballard, 2002) to compute the formation conditions for any phase,
140 the phase present for a given *T* and *P*, hydrate formation *T* and *P* for a given feed composition,
141 formation *T* and *P* for other fluid phases, as well as additional processes such as adiabatic flash
142 or expansion through a turbine. Results for mixed hydrates of CH_4 and various alkanes shows

143 that CSMGem agrees well with laboratory-determined *P*-*T* phase boundary locations to within
144 current experimental uncertainty (Ballard and Sloan, 2004; Luzi et al., 2012). As CSMGem is a
145 proprietary code (although the methods have been published), we use the code interactively to
146 generate the needed datasets—direct linking of CSMGem to TOUGH+HYDRATE was neither
147 possible nor desirable due to the speed considerations discussed above.
148 Two limitations are imposed upon the physical properties investigation. First, we look at
149 sI hydrates only. Allowing for sII or other hydrate structures may extend the usefulness of the
150 relationships to a wider range of systems, but the additional complexity is currently intractable,
151 and in general, hydrates of interest for production are likely to be largely or entirely methane. We
152 also limit our investigation to systems with excess water, again to focus the investigation on
153 systems most likely to be encountered in a reservoir engineering context.
154
155 2.2 Choice of functional forms: novel and complex vs. established and simple
156
157 Our initial attempts at producing fast parametric relationships for the CH_4-CO_2 system
158 used the technique of multiquadrics (MQ) (Hardy, 1990; Kansa, 1990). In this method, a linear
159 combination of functions is used to represent "topographic" data—for example, the *P*-*T*-*x*
160 surface marking a phase boundary in a multicomponent, multiphase system. While this method is
161 extremely powerful and results in simple, easy-to-implement, fast parametric functions, the
162 resulting surfaces fail in terms of the second criteria of Section 1.2. This system, when
163 represented by a MQ expansion fit, would often include slight "waviness" in the interpolation
164 between (*P*, *T*, *x*) points (Seim and Reagan, 2009). While these did not compromise the quality
165 of fit (within the known uncertainty of the fit data), the first and second derivatives of these

variations would be likely to induce large, non-physical effects when used in the simulation framework.

Also considered were simple fits to low- and high-order polynomials. Once again, the smoothness of the derivatives must be considered, even if one can assume that the polynomials converge. For data with simple dependencies (i.e., roughly linear or parabolic due to known factors like inherent physics), this might be sufficient, but much of the thermodynamic data considered here contains various complexities of functional form, such as inflection points, varying curvature, or points of strong curvature or near-discontinuity (i.e., a triple or quadruple point). One subspecies of polynomial that would prove easy to implement would be a power-law formulations or sums of power laws, i.e. $f(x) = f_0 + ax^k$, or $f(x, y) = f_0 + ax^k + by^m$, to represent data with varying curvatures.

When polynomials fail the smoothness test, a last resort is to use splines (Press et al., 1992; Stewart, 1998) to force smoothness of interpolation and smoothness of derivatives. While not as fast as polynomials, tables of data can be pre-processed into arrays of data points, and the first, second, and third derivatives at those points. Efficient Fortran routines exist to quickly interpolate such expressions with O(N) , without the overhead of a full lookup table for all data.

A last set of functions considered are specialized functions—again chosen based on the form of the data—that are known to be (ideally, defined to be) smooth, have smooth derivatives, and that are easily calculated using fast, efficient intrinsic Fortran 95/2003 functions. We have explored the use of incomplete beta functions (von Seggern, 1993) as a means of representing complex curves. However, the data contained in this study, while occasionally exhibiting multiple inflection points and complex types of curvature, is still typically representable by complex *combinations* of otherwise simple functions. Since many of the function vary according

189 to two or more parameters, combinations of simple forms are often easier to fit and implement
190 than elaborate and complex functional forms.
191
192 It should be noted that the choice of form for a given physical property parameterization
193 is essentially determined *ad hoc*, that is, they are selected by hand, and chosen for convenience,
194 speed, and by identifying functional forms that most closely resemble the data as generated by
195 CSMGem. We are not attempting limit ourselves to deriving expressions from first principles,
196 rather, to engineer a practical toolkit that can provide estimates of system properties and fit into
197 the TOUGH+ simulator framework.
198
199 2.3 Curve Fitting
200
201 The bulk of the work in fitting the tables of CSMGem data to various functional forms is
202 performed within the data analysis environment of Igor Pro (Wavemetrics, 2013). Igor Pro takes
203 data in spreadsheet format, organized in a columnar form described as "waves," and allows a
204 wide range of operations to be performed on the data, including for the purposes of this work,
205 curve fitting and 2D plotting. All of the curve fits presented here were performed using version
206 6.x of Igor Pro.
207 In performing these operations, we used a fit metric best described as "keep it simple—
208 for the programmer." As this is not a statistical study to gauge whether laboratory data fits a
209 model, but rather an engineering project to create workable relationships, our goal in each fit was
210 to 1) choose the simplest functional form that can represent the data within the parametric range
211 of interest, 2) insure that the curves intersect the data at each sampled point, 3) insist that the

212 function vary smoothly under *all* circumstances, even if this results in introduction of
213 approximations, and 4) create expressions that can quickly and easily be translated into Fortran
214 or other scientific programming languages, preferably using standard (open source or
215 nonproprietary, readily available) libraries. The smoothness criterion, as mentioned earlier, is
216 essentially non-negotiable for application in the TOUGH+ framework. Thus, we used the
217 internal Igor Pro metrics, including the chi-squared test, to evaluate the relative usefulness of
218 each functional form and the goodness of each individual fit, but the final selection of a
219 particular set of fit parameters was driven primarily by the three points listed above. If additional
220 field or laboratory data becomes available, these fits can be re-evaluated, perhaps with an eye to
221 better matching real-world data. For now, the relationships provide a clean interpolation of
222 CSMGem data in a concise, fast, and easy-to-implement package. Raw data used in the fitting
223 process is available through the online appendix and resources provided by this journal.
224
225 3. Fast parametric functions for key components of the phase diagram
226
227 For all expressions, we use the TOUGH+ unit conventions, where P has units of Pa, T
228 has units of ^{o}C, x (liquid) and Y (gas) are mole fractions. Parametric relationships generated from
229 data reported in other units include the unit conversion to Pa or ^{o}C in the final expression, to
230 preserve the identity of the original data.
231 We separate the properties relationships into two categories—those that require a more
232 complex spline interpolation of data (typically due to the complexity of the shape of the physical
233 properties envelope and/or the necessity of matching data exactly at sampled points), and those
234 that can be simply fit to some combination of polynomials and power-law forms.

235

236 3.1 Cubic splines, or simple functions of cubic splines

237

238 These critical relationships generate quantities that define the fundamental shape of the
239 phase envelope, and accuracy is critical. Therefore, we define the critical locus and phase
240 surfaces by fitting either the data itself (if possible) or the parameters of a series of power-law
241 fits to the data, to a cubic spline.

242 It is not within the scope of this paper to derive the cubic spline, and many good practical
243 references exist to help the user understand the process and program appropriate spline
244 coefficient generators and interpolators (Press et al., 1992; Stewart, 1998). However, we need to
245 define an efficient notation for the purposes of describing the functional forms in Section 3.1. In
246 the following toolkit, we define a cubic spline $S(x)$ as a piecewise function that interpolates a set
247 of (x,y) points, satisfying the conditions:

248 1) $S(x) = S_i(x)$, on the interval $[x_i, x_{i+1}]$ for $i = 0, 1, \ldots, n\text{-}1$;

249 2) $S(x_i) = y_i$ for $i = 0, 1, \ldots, n$; and

250 3) S, S', and S'' are continuous on $[x_0, x_n]$, i.e. S is smooth. This gives us n simple cubic
251 polynomial pieces written as:

252 $$S(x) = S_y(i) + S_b(i)\left(x - S_x(i)\right) + S_c(i)\left(x - S_x(i)\right)^2 + S_d(i)\left(x - S_x(i)\right)^3 \text{ for } i = 0, 1, \ldots, n\text{-}1 \quad (1)$$

253 where S_y, S_b, S_c, and S_d represent $4n$ unknown coefficients and S_x is the vectors of
254 "knots"—i.e. selected values of x. These coefficients are precalculated as part of the curve-fitting
255 exercise, and then interpolation of the actual value of $S(x)$ can be accomplished quickly and
256 cheaply by finding i and evaluating the corresponding sub-polynomial.

257

3.1.1 CH_4-CO_2 hydrate phase diagram

The curves describing hydration pressure, P_H, as a function of composition are critical in defining the mixed CH_4-CO_2 hydrate system, and are described in this section. A series of functions—quadruple-point temperature, critical locus, hydration curves, and VLE curves all form the basis of a workable mixed-hydrate phase diagram. The raw data for the diagram is archived online (through the journal website), and here we present the relationships with the final fitted parameters in place. To ensure accuracy, the parameters were generated by Igor Pro, output in columnar form, and converted via scripts into the formatted equations (and also, into the Fortran code as implemented in TOUGH+BinH), to minimize the chance of transcription errors.

3.1.1.1 Lower quadruple-point temperature

Unlike most hydrate systems, dissolved CO_2 is one of a few species that significantly shifts the freezing point of water, and thus the quadruple point. Therefore composition variations in the CO_2-CH_4 system result in a locus of quadruple points. The lower quadruple points, (P_Q,T_Q), serve as a point of discontinuity within the hydration curve, as the functional form of $P_H(x_{CO2})$ must necessarily change at the transition between (low-P) aqueous-gaseous CO_2-gaseous CH_4 and the (higher-P) region of aqueous-liquid CO_2-gaseous CH_4 coexistence. This transition temperature, which will next be used as a parameter in the generation of the two-part hydration curve, can be represented by a straightforward polynomial:

$$T_Q(x_{CO_2}) = 22.69841897231281 - 8.249662428066445x - 54.09319113815833x^2 + 278.7551606261848x^3 - 649.8072154486597x^4 + 690.4968291527629x^5 - 270.0932037615136x^6 \quad (2)$$

3.1.1.2 Lower hydration curve

The chosen functional form for the hydration curves is illustrated in Figure 1. The two sections of the curve, the first below the quadruple-point temperature (P^{lower}) and the second above the quadruple-point temperature (P^{upper}), are each represented by power-law expressions in T with parameters that vary as functions of x_{CO2}. Each set of P_H vs. T data (above and below the quadruple point) is calculated at a series of constant x_{CO2} values and fit to a power law of the form:

$$P_H(x_{CO_2}) = y + a\left(T^b\right) + c\left(T^d\right) \tag{3}$$

Then, each set of coefficients a, b, c, d are fit to curves as a function of x_{CO2}.

For $P_H{}^{lower}(x_{CO2})$, simple polynomials are sufficient to create smooth curves that intersect the calculated values of the coefficients a, b, c, d:

$$\begin{aligned} La(x_{CO_2}) = {} & 0.1716335619153852 + 1.681663528706526x - 11.17011004409171x^2 \\ & + 39.36670530042825x^3 - 69.93798823331477x^4 + 58.2701693864636x^5 \\ & - 18.23132568623295x^6 \end{aligned} \tag{4}$$

$$\begin{aligned} Lb(x_{CO_2}) = {} & 1.347893452088037 - 3.905631910894871x + 20.88881178467625x^2 \\ & - 67.19629249913626x^3 + 109.903147832899x^4 - 83.88480603423835x^5 \\ & 23.98809793649099x^6 \end{aligned} \tag{5}$$

$$\begin{aligned} Lc(x_{CO_2}) = {} & 7.415168696092792\times10^{-5} + 1.338473767020314\times10^{-4}x \\ & - 7.737972315137834\times10^{-5}x^2 \end{aligned} \tag{6}$$

$$\begin{aligned} Ld(x_{CO_2}) = {} & 2.584503496503497 - 3.360602175602169x + 3.248310023310009x^2 \\ & 1.241064491064483x^3 \end{aligned} \tag{7}$$

Once the coefficients are found, the lower hydration curve, up to the quadruple-point temperature, may be calculated as:

$$P_H^{lower}(x_{CO_2}) = Ly + La\left(T^{Lb}\right) + Lc\left(T^{Ld}\right) \quad \text{where} \quad 0.0 < x < T_Q \tag{8}$$

297 3.1.1.3 Upper hydration curve

298 For $P_H^{upper}(x_{CO2})$, simple polynomials are insufficient to create smooth curves that
299 intersect and smoothly interpolate the computed values of the power-law coefficients *a*, *b*, *c*, *d*.
300 Therefore, we use a combined method. The curve itself is still represented by a power law form,
301 with constant exponents but with the pre-exponential coefficients fit to cubic splines as a
302 function of , as defined in Section 3.1. The 11 knots, corresponding to a set of power-law
303 parameters at x_{CO2} = {0.0, 0.1, 0.2, 0.3, 0.4, 0.5, 0.6, 0.7, 0.8, 0.9, 1.0} and corresponding values
304 and derivatives, are listed in Appendix A for convenience. Using the interpolation method
305 described in Section 3.1 to compute the interval *i* from the vector of knots S_x^U and *x*,

306 $$i\left(x, S_x^U\right) \rightarrow i \tag{9}$$

307 the upper hydrate pressure curve parameters are then calculated as:

308 $$Uy(x_{CO_2}) = S_y^{Uy} + S_b^{Uy}(i)\left(x - S_x^U(i)\right) + S_c^{Uy}(i)\left(x - S_x^U(i)\right)^2 + S_d^{Uy}(i)\left(x - S_x^U(i)\right)^3 \tag{10}$$

309 $$Ua(x_{CO_2}) = S_y^{Ua} + S_b^{Ua}(i)\left(x - S_x^U(i)\right) + S_c^{Ua}(i)\left(x - S_x^U(i)\right)^2 + S_d^{Ua}(i)\left(x - S_x^U(i)\right)^3 \tag{11}$$

310 $$Ub(x_{CO_2}) = S_y^{Ub} + S_b^{Ub}(i)\left(x - S_x^U(i)\right) + S_c^{Ub}(i)\left(x - S_x^U(i)\right)^2 + S_d^{Ub}(i)\left(x - S_x^U(i)\right)^3 \tag{12}$$

311 allowing us to compute the upper hydration pressure curve:

312 $$P_H^{upper}(x_{CO_2}) = Uy + Ua\left(T^{1.5}\right) + Ub\left(T^{2.0}\right) \quad \text{where} \quad T_Q < x < 1.0 \tag{13}$$

313 The two hydration-pressure curves meet at the quadruple point (P_Q, T_Q) (Figure 1), but
314 for all but the lowest values of x_{CO2}, the curves do not smoothly and continuously transition
315 across the connection point. To preserve smoothness in the coupling of the upper and lower
316 curves while allowing minimal inaccuracy, we construct a pair of smoothing functions around T_Q
317 using error functions:

$$MS(x_{CO_2}) = 1.0 + 1000.0 \cdot erfc(100.0 - 100.0x) \quad (14)$$

$$UM(x_{CO_2}) = 0.5erf\left(MS \cdot \left(T - T_Q\right)\right) - 0.5 \quad (15)$$

$$LM(x_{CO_2}) = 0.5erfc\left(MS \cdot \left(T - T_Q\right)\right) \quad (16)$$

Therefore, the hydration pressure at any composition, smoothed, can be represented by:

$$P_H(x_{CO_2}) = LM \cdot P_H^{lower} + UM \cdot P_H^{upper} \quad (17)$$

A sample of the interpolating ability of this expression is illustrated in Figure 2. The complete set of merged and smoothed curves, with quadruple points, is shown in Figure 3 at 0.1 concentration intervals, along with the location of the sI hydrate-stable zone, the approximate location of the liquid and gaseous CO_2 regions outside the hydration zone (roughly below and above P_Q), and how the hydration boundary and quadruple point varies with CO_2 concentration.

3.1.2 Critical locus

Using the definition of cubic spline interpolation in Section 3.1, we process CSMGem data to produce the vectors of 12 knots, values, and derivatives for x_{CO2} ranging from 0.6 to 1.0, since for lower values of x_{CO2}, the vapor-liquid equilibrium zone (VLE) is entirely within the gas hydrate stability zone (GHSZ) where we expect a solid CH_4-CO_2 hydrate phase. As in the previous implementations of cubic splines, we use the interpolation method described in Section 3.1 to compute the interval i from the vector of knots S_x and x,

$$i\left(x, S_x\right) \rightarrow i \quad (18)$$

and the mixture critical pressure may thus be calculated by:

$$P_{crit,mix}(x_{CO_2,mix}) = S_y + S_b(i)\left(x - S_x(i)\right) + S_c(i)\left(x - S_x(i)\right)^2 + S_d(i)\left(x - S_x(i)\right)^3 \quad (19)$$

where $1.0 > x_{CO2,mix} > 0.60$.

For the complementary expression for T_{crit}, the calculated values of critical temperature vs. composition may be represented by a simple polynomial:

$$T_{crit,mix}(x_{CO_2,mix}) = -117.1902467431329+1066.521547692588x^{1.1} - 918.3081766017568x^{1.2} \quad (20)$$

where $1.0 > x_{CO2,mix} > 0.60$. The critical locus is highlighted in blue in Figure 4. Note that for $x_{CO2,mix} < 0.60$, the critical point of the mixture is within the sI hydrate region if hydrate can form (no water limitation), and $T_{crit} < 0^{o}$C.

3.1.3 VLE Saturation curves

Once we have the critical pressure (and critical temperature, see Section 3.2.1), we can begin to describe the 3-D VLE envelope of the binary system. Using CSMGem, we calculate the lower and upper P_{sat} vs. T_{sat} curves as a function of P_{crit}. As the curvature of the P_{sat} vs. T_{sat} data on either side of the critical point is such that a given T may map to two P values (and P_{sat} is at a maximum at T_c), it is more convenient to fit the data as T_{sat} vs. P.

For each of several 2-D slices of the 3-D phase space (slicing across values of x_{CO2}), we fit the curves of T_{sat} vs. P to a power law form:

$$T_{sat,lower}\left(P, P_{crit}(x_{CO_2}), x_{CO_2}\right) = y_0^L(x_{CO_2}) + A^L(x_{CO_2}) \times \left(\frac{P_{crit} - P}{10^6}\right)^{1/2} + B^L(x_{CO_2}) \times \left(\frac{P}{10^6}\right)^{C^L(x_{CO_2})} \quad (21)$$

$$T_{sat,upper}\left(P, P_{crit}(x_{CO_2}), x_{CO_2}\right) = y_0^U(x_{CO_2}) + A^U(x_{CO_2}) \times \left(\frac{P_{crit} - P}{10^6}\right)^{1/2} + B^U(x_{CO_2}) \times \left(\frac{P}{10^6}\right)^{C^U(x_{CO_2})} \quad (22)$$

Determining parameters y_0, A, B, C at each x_{CO2} such that P_{crit} matches for each pair of curves. The dependence of these parameters on x_{CO2} does not lend itself to simple polynomial forms, and therefore to exhibit both smoothness and accuracy at the sampled point, we again interpolate with cubic splines. Choosing eight knots for x_{CO2} (outside of the GHSZ), we create vectors of

values and derivatives to define the cubic splines for each of the parameters (See Appendix A) such that:

$$y_0^L(x_{CO_2}) = S_y^{y0} + S_b^{y0}(i)\left(x - S_x(i)\right) + S_c^{y0}(i)\left(x - S_x(i)\right)^2 + S_d^{y0}(i)\left(x - S_x(i)\right)^3 \quad (23)$$

$$A^L(x_{CO_2}) = S_y^A + S_b^A(i)\left(x - S_x(i)\right) + S_c^A(i)\left(x - S_x(i)\right)^2 + S_d^A(i)\left(x - S_x(i)\right)^3 \quad (24)$$

$$B^L(x_{CO_2}) = S_y^B + S_b^B(i)\left(x - S_x(i)\right) + S_c^B(i)\left(x - S_x(i)\right)^2 + S_d^B(i)\left(x - S_x(i)\right)^3 \quad (25)$$

$$C^L(x_{CO_2}) = S_y^C + S_b^C(i)\left(x - S_x(i)\right) + S_c^C(i)\left(x - S_x(i)\right)^2 + S_d^C(i)\left(x - S_x(i)\right)^3 \quad (26)$$

and:

$$y_0^U(x_{CO_2}) = S_y^{y0} + S_b^{y0}(i)\left(x - S_x(i)\right) + S_c^{y0}(i)\left(x - S_x(i)\right)^2 + S_d^{y0}(i)\left(x - S_x(i)\right)^3 \quad (27)$$

$$A^U(x_{CO_2}) = S_y^A + S_b^A(i)\left(x - S_x(i)\right) + S_c^A(i)\left(x - S_x(i)\right)^2 + S_d^A(i)\left(x - S_x(i)\right)^3 \quad (28)$$

$$B^U(x_{CO_2}) = S_y^B + S_b^B(i)\left(x - S_x(i)\right) + S_c^B(i)\left(x - S_x(i)\right)^2 + S_d^B(i)\left(x - S_x(i)\right)^3 \quad (29)$$

$$C^U(x_{CO_2}) = S_y^C + S_b^C(i)\left(x - S_x(i)\right) + S_c^C(i)\left(x - S_x(i)\right)^2 + S_d^C(i)\left(x - S_x(i)\right)^3 \quad (30)$$

The resulting family of curves defines the phase envelope outside the hydrate stability zone, interpolating the CSMGem data such that the boundaries of the volume can be defined for any (P,T,x) condition. Figure 4 shows several slices of the phase envelope for x_{CO2} = 0.7, 0.8, 0.85, 0.9, 0.95, and 1.0. Note that the curves are smooth, intersect the critical point (a requirement of the spline fits), and coalesce into a single line for pure CO_2. However, a few thermodynamic difficulties (in terms of both modeling and production management in real systems) become apparent. The phase diagram extends over a range of pressures and temperatures that encompass the likely range of operating pressures and temperatures within a permafrost-associated hydrate system subjected to the injection of CO_2 at significant rates. This phase diagram indicates that, as temperature and pressure evolve, regions of the reservoir may

exist in aqueous-gas, aqueous-liquid CO_2-gas, aqueous-supercritical fluid, hydrate-gas, hydrate-aqueous, hydrate-liquid CO_2, hydrate-liquid CO_2-aqueous states. Note that we are seeing slices of a 3-D phase space where many properties are coupled, such that the VLE curves describing the instantaneous state of the system necessarily changes in concert with concentration changes—while concentrations change as hydrate forms or dissociates, phases evolve and disappear, and *P*-*T* changes alter chemical equilibria between phases. This highlights the complexity of the system, and serves as a warning when implementing complex thermodynamics in a simulator context.

Figure 5 shows the complete phase diagram including P_H, the critical locus, and the VLE envelopes for pressures up to 12 MPa. An assessment of this diagram will be performed in section 3.3.

3.2 Other Properties

The following additional properties of the binary system can be represented by polynomials, power-law functions, or power-law functions with parameters fit to polynomial forms. In each case, these derived properties were harvested from the CSMGem program, fit to convenient expressions through the methods described earlier, and the results are presented here. These expressions are valid only through the investigated range of conditions: $P < 12$ MPa (although the data extends to 80 MPa) and $T < 32$ ^{o}C, and the expressions may diverge in unphysical ways outside the stated range. Original data may be examined through the online resources. However, outside these ranges (particular high-*T*), the thermodynamic and phase behavior will be increasing easier to predict using conventional methods. Note that only novel properties, primarily CO_2-related, are described here. Pure methane and methane hydrate

properties are described in the HYDRATE equation-of-state package of the TOUGH+ family of codes (Moridis et al., 2008).

3.2.1 Densities

For density of the CO_2 liquid phase, we first fit the data to create pressure-dependent parameters using simple polynomials:

$$A(P_{liq}) = -6.4988736236065927 + 2.9951749158531462\times10^{-7}P - 6.3881898510082682\times10^{-15}P^2 \quad (31)$$

$$B(P_{liq}) = 1.0893731993111961 + 9.5254531177322741\times10^{-9}P - 7.3920675456387732\times10^{-16}P^2 + 1.2140982621920791\times10^{-23}P^3 \quad (32)$$

$$y_0(P_{liq}) = 898.79334855854381 + 9.5687460221041598\times10^{-6}P - 2.2868869121504460\times10^{-13}P^2 + 2.7601866131215190\times10^{-21}P^3 \quad (32)$$

which are then used to shape a power-law form for density:

$$\rho_{CO_2,liq}(P_{liq},T_{liq}) = y_0(P_{liq}) + A(P_{liq})\times T^{B(P_{liq})} \quad (33)$$

3.2.2 Methane phase equilibria

Gas-phase mole fraction vs. liquid phase mole fraction is also calculated via CSMGem and fits to a simple power-law form:

$$Y_{CH_4}(x_{CH_4}) = 1.11106721025438\, x^{1.3695} \quad (34)$$

3.2.3 Heat capacities

Heat capacities of liquid CO_2 are most conveniently fit to a power-law form in T, with pressure dependent parameters described via simple polynomials:

$$A(P_{liq}) = 2.1670238871063212 - 3.6214160370115135\times10^{-7}P + 2.5712819297978501\times10^{-14}P^2 - 8.2207649831525329\times10^{-22}P^3 + 9.6828167007265819\times10^{-30}P^4 \quad (35)$$

$$B(P_{liq}) = 1.4689866130279257 - 1.7060827005377455\times10^{-8}P + 1.9224893097696102\times10^{-16}P^2 \quad (36)$$

$$y_0(P_{liq}) = 115.90286947473265 - 2.3407325547425592\times10^{-6}P + 4.0314371148066704\times10^{-14}P^2 \quad (37)$$

$$Cp_{CO_2,liq}(P_{liq},T_{liq}) = y_0(P_{liq}) + B(P_{liq})\times T^{B(P_{liq})} \quad (38)$$

3.2.4 Thermal conductivities

The thermal conductivity of liquid CO_2 may similarly be represented, with temperature dependent parameters controlled a power-law expression in P:

$$A(T_{liq}) = -7.8579044050122865\times10^{-3} + 5.5394710718504299\times10^{-3}T - 6.2929748865142208\times10^{-4}T^2 + 1.9060028896215096\times10^{-5}T^3 \quad (39)$$

$$B(T_{liq}) = 0.74520450096844948 + 3.1526443778506458\times10^{-3}T - 2.5164621737342511\times10^{-3}T^2 + 9.7444027088786222\times10^{-5}T^3 - 1.3337735750482373\times10^{-6}T^4 \quad (40)$$

$$y_0(T_{liq}) = 0.11853632077933009 - 7.6586100389543889\times10^{-3}T + 6.8576404138889703\times10^{-4}T^2 - 2.2434324176145396\times10^{-5}T^3 \quad (41)$$

$$\kappa_{CO_2,liq}(P_{liq},T_{liq}) = y_0(T_{liq}) + A(T_{liq})\times\left(\frac{P}{10^5} - 35.0\right)^{B(T_{liq})} \quad (42)$$

3.2.5 Enthalpies

Enthalpies of liquid CO_2 may be described in the same fashion:

$$A(T_{liq}) = 6.8922373855486381\text{-}7.4944873020148099\text{T-}0.42407562184666392T^2 + 3.1434245395365421\times10^{-2}T^3 - 1.1110460840569548\times10^{-3}T^4 + 1.5063125985170777\times10^{-5}T^5 \quad (43)$$

$$B(T_{liq}) = \text{-}7.0753126628472024\times10^{-2} + 8.5007373669959731\times10^{-3}T - 3.7250751496378199\times10^{-3}T^2 + 1.9770700452401366\times10^{-4}T^3 - 4.2502200308654369\times10^{-6}T^4 \quad (44)$$

$$y_0(T_{liq}) = 0.11853632077933009 - 7.6586100389543889\times10^{-3}T + 6.8576404138889703\times10^{-4}T^2 - 2.2434324176145396\times10^{-2}T^3 \quad (45)$$

$$H_{CO_2,liq}(P_{liq},T_{liq}) = y_0(T_{liq}) + A(T_{liq})\times\left(\frac{P}{10^5} - 30.0\right)^{B(T_{liq})} \quad (46)$$

3.2.6 Viscosities

Viscosity of liquid CO_2 may also use this form:

$$A(T_{liq}) = 194.47399566335787\text{-}276.23497588809352T + 100.73462527792871T^2 - 15.2545504818204 40T^3 + 1.1088306087554245T^4 - 3.8309820806714766\times10^{-2}T^5 + 5.0508243207209285\times10^{-4}T^6 \quad (47)$$

$$B(T_{liq}) = 0.77947264848861364 + 8.7862026724561271\times10^{-3}T - 3.7364594467981928\times10^{-3}T^2 + 1.8285005907721914\times10^{-4}T^3 - 3.1838465124297668\times10^{-6}T^4 \quad (48)$$

$$y_0(T_{liq}) = 903.59752929883086 + 284.91889111950320T - 110.50532839691671T^2 + 16.568405839893483T^3 - 1.1971697407203625T^4 + 4.1156481746371522\times10^{-2}T^5 - 5.4075637696365732\times10^{-4}T^6 \quad (49)$$

$$\mu_{CO_2,liq}(P,T) = y_0(T_{liq}) + A(T_{liq})\times\left(\frac{P}{10^5} - 40.0\right)^{B(T_{liq})} \quad (50)$$

447 3.2.7 Implementation

448 The primary and secondary physical-properties expressions have been implemented as
449 part of the BinH equation of state module for TOUGH+. TOUGH+BinH is currently a research
450 code, and not part of the standard licensed suite of TOUGH+ codes found on the LBNL tech
451 transfer website (*http://esd.lbl.gov/research/projects/tough/licensing/*). However, we direct
452 questions from interested researchers to the authors of this paper. Future plans include expanding
453 the existing set of LBNL/Earth Science physical properties tools (*http://esdtools.lbl.gov/gaseos*)
454 to include the BinH properties modules. A description of the TOUGH+BinH code and its
455 validation using both simple and complex mixed-hydrate problems will be presented in a
456 forthcoming paper.

457

458 3.3 The complete phase diagram

459 Figure 5 shows the complete phase diagram including P_H, the critical locus, and the VLE
460 envelopes for pressures up to 12 MPa. Note again that we are presenting multiple slices of 3-D
461 phase envelopes on a single plot. To clarify this, Figure 6 presents the same phase diagram in six
462 panels, for single values of x_{CO2}: 0.0, 0.6, 0.7, 0.8, 0.9, and 1.0, in order to illustrate the geometry
463 of the individual 2D slices that comprise the 3D phase envelope that is represented in Figure 5.

464 Thus, the hydration pressure curves, in red, and the upper and lower curves for saturation
465 temperature/pressure are actually cross-sections of 3-D surfaces, with the critical loci forming a
466 critical curve that extends across the top of the volume generated by the VLE envelope. The
467 upper and lower (in P) saturation curves also form enclosed volumes, with the critical locus as
468 the upper/rightmost (high-T, high-P) seam of the volume. These surfaces and volumes are
469 bounded in the third dimension (x_{CO2}) by the pure-CH_4 and pure CO_2 phase diagrams, $x = 1.0$

and $x = 0.0$. Also note the hydration curve (2-D slice) for $x = 0.4$ (Figure 5) which serves roughly as an upper-T limit of the hydration surface.

Several other regions of interest are identified in Figures 5 and 6. First, to the lower right, below the phase envelopes and to the right of the hydration curve, is an aqueous-gas region. Second, above the phase envelopes, to the right of the hydration curves, is an aqueous-condensed fluid zone, with the fluid being supercritical to the right of the mixture critical point and subcritical to the left (above the critical pressure, the subcritical to supercritical transition is smooth and continuous). Note that a system that follows a P-T path that travels past the mixture critical point in T, moves upward through increased pressure, and then moves left due to a decrease in T could actually skirt the gas-liquid phase transition zone and move from gas to liquid/fluid without a discrete phase transition. Note also that the critical locus places the location of such a potential transition within the reasonable range of hydrate reservoir conditions at CO_2 concentrations of 70% to 80%.

Also highlighted, by an orange strip, is the approximately P-T range of the Ignik Sikumi field test. While it is clear that such a system is very stable with regard to CO_2-bearing hydrates (and thus a good candidate for a sequestration test), it is also clear that any field test involving injection of warm CO_2-bearing fluids certainly risks an excursion into the thermodynamically complex zones in the center of the phase diagram. The simulation of complex regimes with mixed hydrates, multiple fluid phases, and the possible entrance of the near-critical region is likely to be a challenging problem. The fast parametric relationships described here allow this problem to be understood, such that the investigation can identify complex regimes and thus comprehend the potential difficulties of simulating the process.

4. Conclusions

The use of these expressions in a reservoir simulation will be described in subsequent publications. However, the mere exploration of the data space and the gathering, fitting, plotting, and attempts to understand the data reveal a system that is extremely complex, and these investigations have already extended understanding of the system beyond what has been described in the literature.

Key observations include:

1) The mixed-hydrate phase behavior is poorly constrained by data, therefore speed was chosen over fidelity. While incorporation of *ab initio*-style methods directly into simulator leads to the greatest flexibility, with the creation of detailed look-up tables close behind in this regard, such methods limit the extent of the simulated system due to the computational overhead for operations that may be performed thousands or millions of times within a simulation cycle. More recent work in methane hydrate simulation by this group, including (Reagan et. al, 2015; Moridis et al., 2013; Reagan et. al, 2010) has demonstrated the need to simulate large, complex, heterogeneous, geologically realistic, and often three-dimensional systems. Such simulations require highly efficient physical properties relationships. While these relationships are limited by the necessarily simplicity of the functional forms, it is important to recognize that the underlying dataset is itself derived from a model. Such model-derived properties have a maximum of the accuracy or realism (or at least a limit to the certainty), therefore it is clear that *ad hoc* fast parametric relationships are a fair, efficient, and sufficient means by which to represent the data. As additional field and laboratory data is gathered, these relationships can be updated and evaluated for accuracy and realism.

2) These physical properties relationships must be used carefully and results must be evaluated according to physical knowledge and likely system behavior. The most important product of this research is an understanding of the complexity of the CO_2-CH_4 hydrate system. It is not merely an interpolation of single-component phase diagrams—the second component results in additional degrees of freedom, new liquid phases, and the need to represent phase boundaries as surfaces and volumes.

3) A direct consequence of (2) is that the phase behavior will be actively coupled to changes in concentration in addition to changes in *P* and *T*. For example, during hydrate formation, the hydration phase boundary *and* the composition of the formed hydrate is dependent on the concentration of CO_2 and CH_4 in the aqueous phase, but subsequent removal of CH_4 and CO_2 from the aqueous phase (not in 1:1 proportion) will move a simulated grid element into a difference slice of the phase diagram in the *x*-dimension as well as in *P*-*T* space. This creates a new question for reservoir simulators—whether each element retains a history of hydrate formation and dissociation along with the relation concentration changes, or whether some averaging assumption is used to create a hysteretic process of formation-dissociation in mixed systems. The practical numerical consequences of this have not fully been explored.

4) This understanding will be tested and validated by future analyses of the Ignik Sikumi test results. Although the 2012 field test went beyond the parameters originally proposed as this research began—particularly in the use of injected N_2 for flow assurance—the data gathered shows, in preliminary analysis, evidence that the exchange reactions occurred *in situ*, and the BinH physical properties package will be validated against the available data and extended in necessary. However, it is unlikely that the N_2 component can be added to the parameterized

phase diagram, due to the order-of-magnitude increase in complexity beyond the 3D-phase diagram presented here. Future publications by this group and others will explore this area.

For now, we present this first simple, concise, easy-to-implement set of fast parametric relationships for mixed CO_2-CH_4 hydrate systems.

5. Acknowledgements

The authors thank Katie S. Seim for her extensive (and quite grueling) work generating the data sets from the CSMGem application and her work in exploring the use of multiquadrics. Her work was funded by the DOE Pre-Service Teacher/CSEE summer program at LBNL. The work of developing the physical property relationships, as well as the development of the BinH EOS module, the TOUGH+BinH code, and subsequent work, was funded by ConocoPhillips.

6. References

Anderson, B.J., Bazant, M.Z., Tester, M.Z., Tester, J.W., Trout, B.L., "Application of the Cell Potential Method To Predict Phase Equilibria of Multicomponent Gas Hydrate Systems," J. Phys. Chem. B., 109, 8153-8163, 2005.

Ballard, A.L., 2002. A Non-Ideal Hydrate Solid Solution Model for a Multiphase Equilibria Program. Ph.D Thesis, Colorado School of Mines, Golden, CO.

Ballard, A.L., Sloan, E.D., 2004. The next generation of hydrate prediction IV: A comparison of available hydrate prediction programs. Fluid Phase Eq. 216, 257-270.

559 Donnelly, H.G., Katz, D.L., 1954. Phase Equilibria in the Carbon Dioxide-Methane System. Ind.
560 Eng. Chem. 46, 3, 511-517.
561 Garapati, N., Velaga, S., Anderson, B.J., "Development Of A Thermodynamic Framework For
562 The Simulation Of Mixed Gas Hydrates: Formation, Dissociation And CO2-CH4
563 Exchange," *Proc.* 7th International Conference on Gas Hydrates (ICGH-2011),
564 Edinburgh, July 17-21, 2011.
565 Gupta, A.K., Ph.D. Thesis, University of Calgary, 1990.
566 Hardy, R.L., 1990. Theory and Applications of the Multiquadric-Biharmonic Method.
567 Computers Math. Applic. 19 (8-9), 163-208.
568 Hester, K.C., Stevens, J.C., Howard, J.J., "Composition Studies to Determine Rate and Extent of
569 CO2 Exchange in a Hydrate-Bearing Core," *Proc.* 7th International Conference on Gas
570 Hydrates (ICGH-2011), Edinburgh, July 17-21, 2011.
571 Howard, J., Hester, K., Stevens, J., and Rydzy, M., "Ultrasonic velocity measurements during
572 experimental CH4 hydrate formation and CO2 exchange," *Proc.* 7th International
573 Conference on Gas Hydrates (ICGH-2011), Edinburgh, July 17-21, 2011.
574 Kansa, E.J., 1990. Multiquadrics—A Scattered Data Approximately Scheme with Applications
575 to Computional Fluid Dynamics—I. Surface Approximations and Partial Derivative
576 Estimates. Computers Math. Applic. 19 (8-9), 127-145.
577 Luzi, M., Schicks, J.M., Naumann, R., Erzinger, J., "Systematic kinetic studies on mixed gas
578 hydrates by Raman spectroscopy and powder X-ray diffraction," J. Chem.
579 Thermodynamics, 43, 28-35, doi:10.1016/j.jct.2011.12.004, 2012.
580 Moridis, G.J., Kowalsky, M., Pruess, K. TOUGH+HYDRATE Users Manual, Lawrence
581 Berkeley National Laboratory, Berkeley, CA, 2008.

582 Moridis, G.J., Collett, T.S., Pooladi-Darwish, M., Hancock, S., Santamarina, C., Boswell, R.,
583 Kneafsey, T., Rutqvist, J., Kowalsky, M.J., Reagan, M.T., Sloan, E.D., Sum, A.K., Koh,
584 C. Challenges, Uncertainties and Issues Facing Gas Production From Hydrate Deposits in
585 Geologic Systems. SPE Res. Eval. & Eng, 14, 1, 76-112, 2011.
586 Moridis, G.J., Kim, J., Reagan, M.T., Kim, S.J. Feasibility of Gas Production from a Gas
587 Hydrate Accumulation at the UBGH2-6 Site of the Ulleung Basin in the Korean East Sea,
588 J. Pet. Sci. Eng., doi: 10.1016/j.petrol.2013.03.002, 2013.
589 NETL, 2012 Ignik Sikumi Gas Hydrate Field Trial, http://www.netl.doe.gov/technologies/oil-
590 gas/FutureSupply/MethaneHydrates/rd-program/ANSWell/co2_ch4exchange.html, 2013.
591 Press, W.H., Teukolsky, S.A., Vetterling, W.T., Flannery, B.P., 1992. Numerical Recipes in
592 Fortran 77, 2nd Ed., Cambridge Univ. Press, New York, NY.
593 Pruess, K., ECO2M: A TOUGH2 Fluid Property Module for Mixtures of Water, NaCl, and CO2,
594 Including Super- and Sub-Critical Conditions, and Phase Change Between Liquid and
595 Gaseous CO2, LBNL-4590, Lawrence Berkeley National Laboratory, Berkeley, CA,
596 2011.
597 Reagan, M.T., Kowalsky, M.B., Moridis, G.J., Silpngarmlert, S., "The Effect of Reservoir
598 Heterogeneity on Gas Production From Hydrate Accumulations in the Permafrost," SPE
599 132649, LBNL-3981E, *Proc*. 2010 SPE Western North American Regional Meeting,
600 Anaheim, California, 27-29 May 2010.
601 Reagan, M.T., Moridis, G.J., Freeman, C.M., Pan, L., Boyle, K.L., Keen, N., Husebo, J.A.,
602 "Field-Scale Simulation of Production from Oceanic Gas Hydrate Deposits," *Transport*
603 *in Porous Media*, 108(1), 151-169, 2015.

Schoderbek, D., Farrel, H., Hester, K., Howard, J.,Ratterman, K., Silpngarmlert, S.,Martin, K.L., Smith, B., Klein, P. "ConocoPhillips Gas Hydrate Production Test Final Technical Report,' July 20, 2013, http://www.netl.doe.gov/File%20Library/Research/Oil-Gas/methane%20hydrates/nt0006553-final-report-hydrates.pdf.

Seim, K.S., Reagan, M.T., "Multiquadratic Representation of Complex Phase Behavior for the Mixed CO2-CH4 Hydrate System", *Proc.* LBNL CSEE symposium, Berkeley, CA, August, 2009.

Sloan, E.D., Koh, C. 2008. Clathrate Hydrates of Natural Gases, 3rd ed., Publisher, New York, pages.

Stewart, G.W. 1998. Lecture on Advanced Numerical Analysis, SIAM, Philadelphia, PA.

Van der Waals, J. H., Platteeuw, J. C., Adv. Chem. Phys., 2, 1– 57, 1959.

Von Seggern, D. 1993. CRC Standard Curves and Surfaces, 2nd Ed., CRC Press Inc., Boca Raton, FL.

White, M. D.; M. Oostrom. STOMP Subsurface Transport Over Multiple Phase: User's Guide PNNL-15782 (UC-2010). Pacific Northwest National Laboratory, Richland, Washington, 2006.

White, M.D., Wurstner, S.K., McGrail, B.P. Numerical studies of methane production from Class 1gas hydrate accumulations enhanced with Carbon dioxide injection. Marine and Petroleum Geology. 2011, 28(2), 546-560.

626

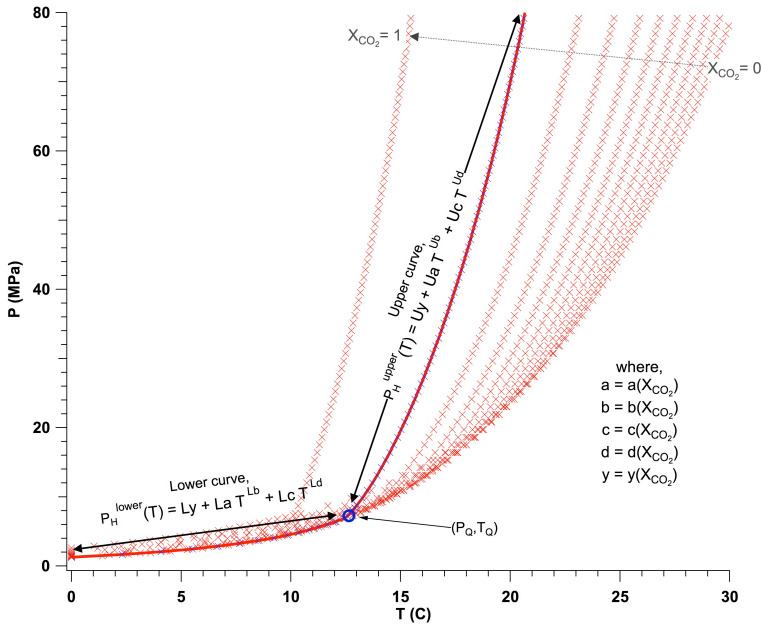

627

628 Figure 1: Illustration of the upper and lower hydration curves (red lines) intersecting at a
629 quadruple point (P_Q,T_Q) (blue circle) overlaid upon the set of raw $P_H(x_{CO2},T)$ data generated by
630 CSMGem (Xs).

631

632

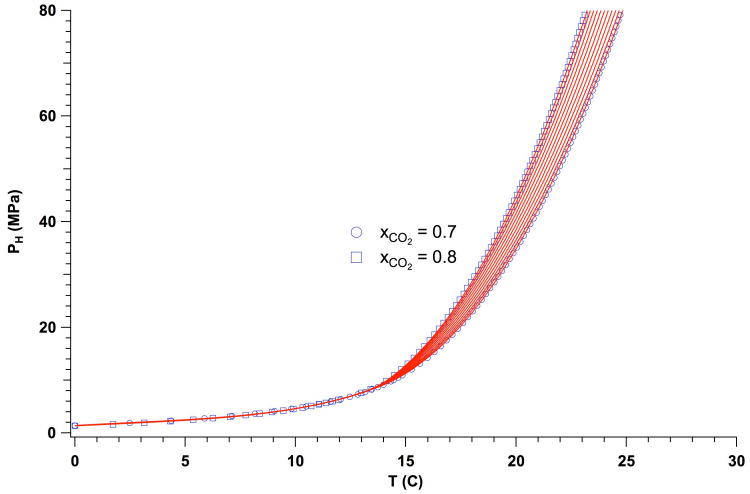

Figure 2: Demonstration of the interpolation ability of the combined spline-power law representation of P_H. CSMGem data points are shown as blue symbols for x_{CO2} = 0.7 and 0.8, while $P_H(x_{CO2})$ as represented by the smooth parametric relationship is show in red for in 0.01 intervals.

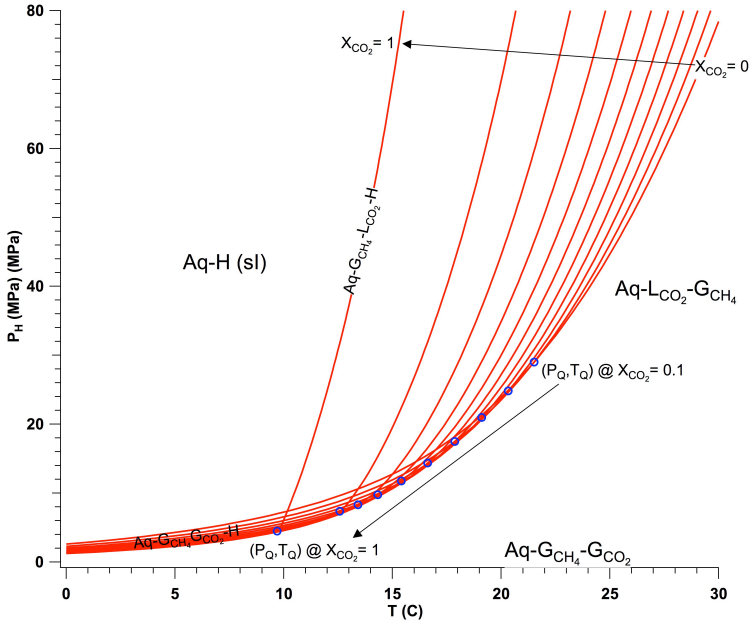

Figure 3: Set of spline-power law curves for the upper and low P_H curve fits, showing the approximate location of liquid and gaseous CO_2 zones (above and below the quadruple point), the sI hydrate zone, and variation with x_{CO2}.

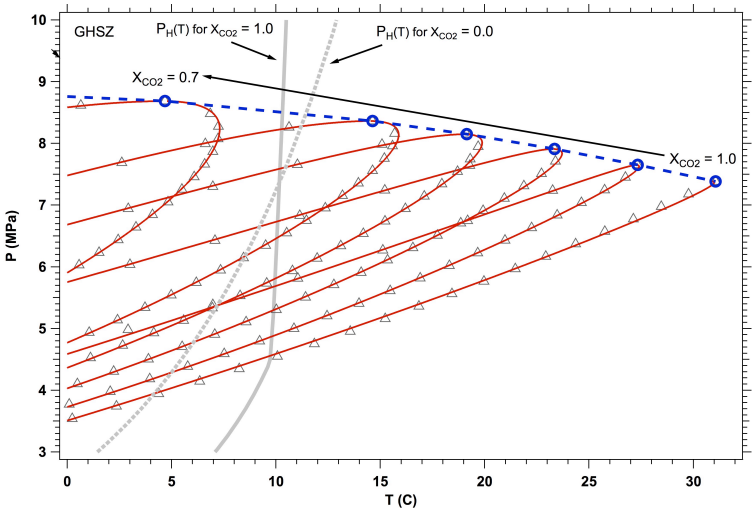

Figure 4: T_{sat} vs. P_{sat} for a range of x_{CO2} from 0.7 to 1.0. CSMGem data are gray points, red lines are the parametric functions derived from the data, and the critical locus is in blue. The hydration curves for x_{CO2} = 1.0 and x_{CO2} = 0.0 are also indicated to show the varying transition line between the GHSZ and the multiphase CH_4-CO_2-aqueous regions.

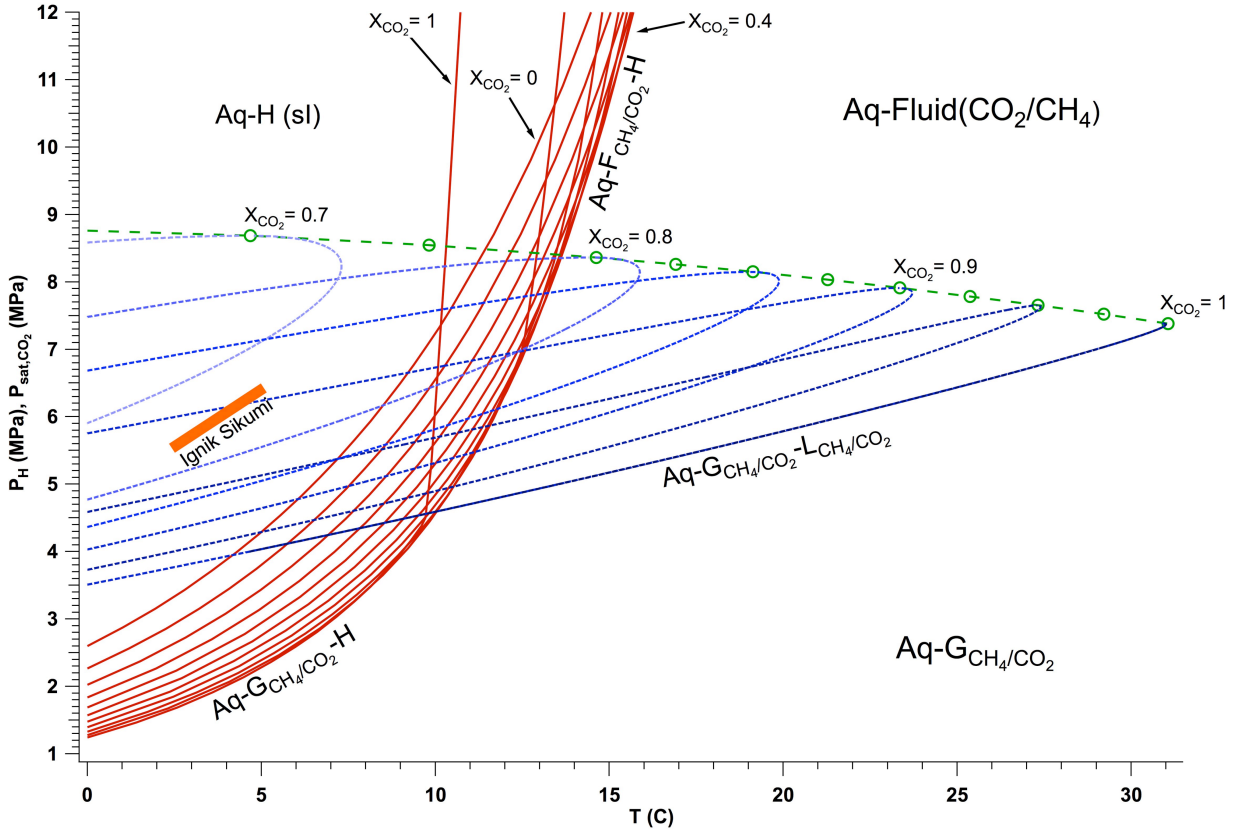

Figure 5: Phase diagram for the CO_2-CH_4 hydrate system. Hydration pressure curves are in red, VLE phase envelopes in blue, the critical locus in green, and the approximate *P*-*T* space for the Ignik Sikumi reservoir is marked in orange.

662

663

664

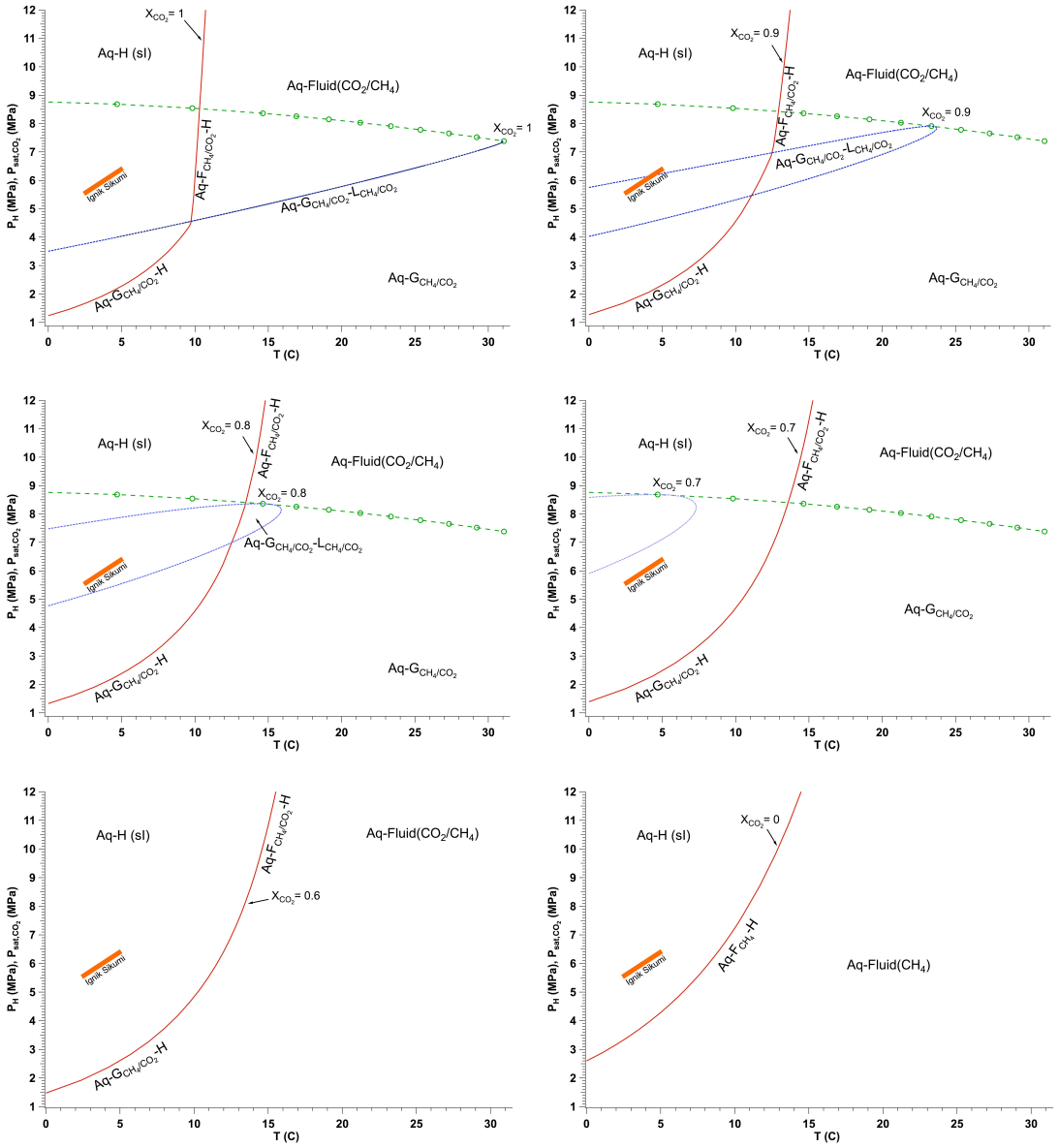

665 Figure 6: Phase diagrams for the CO_2-CH_4 hydrate system, at selected single values of x_{CO2}.
666 Hydration pressure curves are in red, VLE phase envelopes in blue, the critical locus (when
667 relevant) in green, and the approximate *P*-*T* space for the Ignik Sikumi reservoir is marked in
668 orange.

669

Appendix A: Vectors of cubic spline parameters

3.1.1.3 $P_h^{upper}(x_{CO2})$

S_x = { 0.0, 0.1, 0.2, 0.3, 0.4, 0.5, 0.6, 0.7, 0.8, 0.9, 1.0 }

S_y^{Uy} = { 44.540802205791, 47.194620682007, 47.418637801017, 47.238773097740,
46.483681230367, 45.497887865020, 45.020000607331, 44.252445392531,
43.870589467427, 38.591601938069, 20.484870944437 }

S_b^{Uy} = { 46.0809033265, 10.3719987559, -1.23383049348, -4.11210430996,
-10.3664493863, -6.64865512624, -6.94934879957, -2.91722385012,
-15.8640899970, -103.451719795, -271.900586510 }

S_c^{Uy} = { -229.1925112262, -127.8965344803, 11.83824198625, -40.62098015098,
-21.92247061287, 59.10041321388, -62.10734994721, 102.4285994417,
-231.8972609110, -643.9790370740, -1040.50963007 }

S_d^{Uy} = { 337.6532558195, 465.7825882220, -174.8640737908, 62.32836512704,
270.0762794225, -404.0258772036, 548.4531646300, -1114.419534509,
-1373.605920543, -1321.768643336, -1321.768643336 }

S_y^{Ua} = { -2.144067539313, -2.390018043677, -2.561046481243, -2.719739488264,
-2.867329294068, -3.026885481117, -3.248306619803, -3.545521805380,
-4.040042256155, -4.72099850490, -6.167211750641 }

S_b^{Ua} = { -3.060754328082, -1.962566819605, -1.598346651396, -1.535689912412,
-1.447378083698, -1.889177538412, -2.425231534688, -3.968986050716,
-5.450893353028, -9.491741522785, -20.39722539038 }

S_c^{Ua} = { 7.055603448658, 3.926271636118, -0.2840699540319, 0.9106373438693,
-0.027519056720, -4.390475490419, -0.9700644723457, -14.46748068793,
-0.351592335176, -40.05688936239, -68.997949313614 }

S_d^{Ua} = { -10.43110604180, -14.03447196716, 3.982357659671, -3.127188001966,
-14.54318811233, 11.40137006024, -44.99138738530, 47.05296117586,
-132.3509900907, -96.47019983740, -96.47019983740 }

S_y^{Ub} = { 0.429010783418, 0.476201872159, 0.513666328255, 0.550738619151,
0.588199766283, 0.630742709757, 0.688620015725, 0.769327916966,
0.905326912506, 1.13361139367, 1.809597021278 }

S_b^{Ub} = { 0.554181967705, 0.405197252854, 0.364695365969, 0.372123693015,
0.382813002808, 0.496747013926, 0.642806424741, 1.089583503368,
1.500066465217, 3.838654937081, 10.27341704963 }

S_c^{Ub} = { -0.978285260403, -0.511561888112, 0.106543019270, -0.0322597488124,
0.139152846742, 1.000187264431, 0.460406843721, 4.0073639425477,
0.097465675947, 23.28841904269, 41.05920208276 }

S_d^{Ub} = { 1.555744574300, 2.060349691278, -0.4626758936107, 0.5713753185165,
2.870114725628, -1.799268069031, 11.82319032942, -13.03299422200,
77.30317788915, 59.23594346692, 59.23594346692 }

3.1.2 $P_{crit,mix}(T)$

S_x = { 0.60, 0.65, 0.70, 0.75, 0.80, 0.85, 0.875, 0.90, 0.925, 0.95, 0.975, 1.00 }

S_y = { 8.7967996597290, 8.7739000320435, 8.6856002807617, 8.5450000762939,
8.3632001876831, 8.1492996215820, 8.0326995849609, 7.9107999801636,
7.7842998504639, 7.6538000106812, 7.5198998451233, 7.3831000328064 }

S_b = { 0.28422486890644, -1.1565444082945, -2.3300099737657, -3.2574130416134,
-3.9843434444976, -4.5472404631112, -4.7751282659811, -4.9722034431794,
-5.1440261009498, -5.2916884909120, -5.4172205762715, -5.5234265489726 }

S_c = { -15.717659813025, -13.097725730993, -10.371585578432, -8.1764757785213,
-6.3621322791625, -4.8958080931104, -4.2197040216835, -3.6633030662495,
-3.2096032445686, -2.6968923539163, -2.3243910604667, -1.9238478475765 }

S_d = { 17.466227213542, 18.174267683744, 14.634065332737, 12.095623329059,
9.7754945736810, 9.0147209523586, 7.4186794057867, 6.0493309557444,
6.8361452086983, 4.9666839126616, 5.3405761718689, 5.3405761718689 }

3.1.3 $T_{sat}(P, P_{crit}, x_{CO2})$

3.1.3.1 $T_{sat,lower}(P, P_{crit}, x_{CO2})$

S_x = { 0.70, 0.80, 0.85, 0.90, 0.925, 0.95, 0.975, 1.00 }

For $y_0^L(x_{CO2})$:

$S_y^{y0} = \{$ -149.50999450684, -129.61700439453, -116.00000000000, -103.08000183105,
-82.971801757812, -61.752799987793, -57.365299224854, -56.712398529053 $\}$

$S_b^{y0} = \{$ -353.13337879513, 529.41936919226, 547.97287490418, 463.12943880822,
432.56918228372, 286.22594265260, 88.107725553651, -33.808669818381 $\}$

$S_c^{y0} = \{$ 7736.3709176714, 1089.1565622025, -347.01633372566, -3046.7211101126,
2435.5159796226, -5362.3807722450, -2562.3479117131, -2314.3079031682 $\}$

$S_d^{y0} = \{$ -22157.381184896, -19148.971945709, -35996.063685160, 36548.247264902,
–51985.978345784, 37333.771473758, 3307.2001139325, 3307.2001139325 $\}$

For $A^L(x_{CO2})$:

$S_y^A = \{$ -13.363599777222, -9.4989995956421, -7.7455401420593, -6.0714201927185,
-2.8874299526215, -1.2684899568558, 0.050986301153898, 2.0000000000000 $\}$

$S_b^A = \{$ -13.559678649381, 69.824308013394, 68.228785420640, 68.570078654879,
44.950159477069, 39.805097588610, 65.014978329767, 92.353783915013 $\}$

$S_c^A = \{$ 732.33054732756, 101.50931930019, -165.33022301037, 178.98195237993,
-651.38033593613, 548.47909816694, 459.91613147936, 633.63609193048 $\}$

$S_d^A = \{$ -2102.7374267579, -3557.8605641409, 4590.8290052041, -5535.7485887737,
7999.0628940205, -1180.8395558345, 2316.2661393484, 2316.2661393484 $\}$

For $B^L(x_{CO2})$:

$S_y^B = \{$ 86.607398986816, 67.680198669434, 54.000000000000, 42.069000244141,
29.501199722290, 23.901399612427, 22.854700088501, 22.440200805664 $\}$

$S_b^B = \{$ 451.40132523918, -545.75555294100, -532.03929166971, -399.43109141533,
-156.84284088587, -63.253582944022, -25.415776891991, -10.427166299537 $\}$

S_c^B = { -9248.6310705885, -722.93771121332, 1271.5881620650, 4032.7398481100, 819.02516247926, 1052.7599963577, 460.75224572358, 138.79217797456 }

S_d^B = { 28418.977864584, 26593.678310377, 36815.355813934, -21424.764570872, 1558.2322258561, -7893.4366751212, -4292.8009033203, -4292.8009033203 }

For $C^L(x_{CO2})$:

S_y^C = { 0.26699998974800, 0.35600000619888, 0.42617699503899, 0.50800001621246, 0.61945998668671, 0.64627200365067, 0.66000002622604, 0.68117702007294 }

S_b^C = { -1.1055035337768, 2.4841832463902, 3.1546565516628, 3.1371917485884, 1.1926597152332, 0.38848863677098, 0.68992745003464, 1.0404035337631 }

S_c^C = { 23.968243146898, 11.928624654771, 14.890307556133, -15.588899679108, -23.301740987996, 7.2183194187524, 4.8392331117939, 9.1798102373433 }

S_d^C = { -40.132061640424, 39.489105351485, -406.38942980320, -51.418942059258, 203.46706937833, -31.721150759446, 57.874361673991, 57.874361673991 }

3.1.3.2 $T_{sat,upper}(P, P_{crit}, x_{CO2})$

S_x = { 0.70, 0.80, 0.85, 0.90, 0.925, 0.95, 0.975, 1.00 }

For ${y_0}^U(x_{CO2})$:

S_y^{y0} = { -126.44499969482, -97.731597900391, -92.495498657227, -87.336402893066, -83.302803039551, -81.411201477051, -70.891700744629, -56.712398529053 }

S_b^{y0} = { 494.27800768209, 140.02400444356, 77.655964334629, 173.06383865738, 80.785357207229, 214.81890243558, 549.27130844107, 551.95221755991 }

S_c^{y0} = { -2671.7796597474, -870.76037263799, -376.60042954056, -2284.7579159955, -5975.8971740015, 11337.238983136, 2040.8572570838, -1933.6208923303 }

745 S_d^{y0} = { 6003.3976236979, 3294.3996206495, 17742.388970241, -110142.06786663, 230841.81542850, -123951.75634736, -52993.041992188, -52993.041992188 }

746

747 For $A^U(x_{CO2})$:

748 S_y^A = { 7.9442000389099, 5.9846801757812, 4.8447499275208, 3.6849999427795, 2.7475900650024, 2.2245700359344, 1.5733000040054, 2.0000000000000 }

749 S_b^A = { -14.673955225174, -23.646837290899, -19.511123357277, -36.289483260095, -28.657673416565, -24.331411895058, -14.931486322846, 57.108952874309 }

750

751 S_c^A = { -57.908481526133, -31.820339131112, 114.53461780354, -450.10181585989, 755.37420960110, -582.32374874082, 958.32077162927, 1923.2967962569 }

752

753 S_d^A = { 86.960474650069, 975.69971289767 -3764.2428910895, 16073.013672813, -17835.972777892, 20541.926938268, 12866.346995036, 12866.346995036 }

754

755 For $B^U(x_{CO2})$:

756 S_y^B = { 57.721000671387, 41.733898162842, 41.496398925781, 41.117698669434, 41.099998474121, 41.000000000000, 34.741500854492, 22.440200805664 }

757 S_b^B = { -345.46418320498, -27.396890606866, 0.86627157128403, -13.040165282762, 25.202328934714, -101.89299078812, -380.65008013768, -602.68259198146 }

758

759 S_c^B = { 2387.1218176048, 793.55110837632, -228.28786481331, -49.840872267607, 1579.5406409666, -6663.3534298802, -4486.9301441021, -4394.3703296489 }

760

761 S_d^B = { -5311.9023640950, -6812.2598212642, 1189.6466169714, 21725.086843123, -109905.25427796, 29018.977143708, 1234.1308593751, 1234.1308593751 }

762

763 For $C^U(x_{CO2})$:

764 S_y^C = { 0.37927299737930, 0.46559700369835, 0.47099998593330, 0.47814500331879, 0.47349500656128, 0.47875100374222, 0.52399998903275, 0.68117702007294 }

765

$$S_b^C = \{\ 1.8144867943976,\ 0.18114048965238,\ 0.16837416272703,\ -0.10175716333424,$$
$$-0.12256468069718,\ 0.66473593693475,\ 3.5242188295341,\ 9.5295107046150\ \}$$

$$S_c^C = \{\ -12.203938888762,\ -4.1295241586901,\ 3.8741976201830,\ -9.2768241414084,$$
$$8.4445234468908,\ 23.047501258387,\ 91.331814445588,\ 148.87986055765\ \}$$

$$S_d^C = \{\ 26.914715766907,\ 53.358145192487,\ -87.673478410610,\ 236.28463451066,$$
$$194.70637081994,\ 910.45750916269,\ 767.30728149414,\ 767.30728149414\ \}$$